Thiol Ligation of Two Zinc Atoms to a Class I tRNA Synthetase: Evidence for Unshared Thiols and Role in Amino Acid Binding and Utilization†

James A. Landro, Eric Schmidt, and Paul Schimmel*

Department of Biology, Massachusetts Institute of Technology, Cambridge, Massachusetts 02139

David L. Tierney and James E. Penner-Hahn*

Department of Chemistry, University of Michigan, Ann Arbor, Michigan 48109

Received June 15, 1994; Revised Manuscript Received September 12, 1994⊗

ABSTRACT: Class I tRNA synthetases generally contain a characteristic N-terminal catalytic core joined to a C-terminal domain that is idiosyncratic to the enzyme. The closely related class I *Escherichia coli* methionyl- and isoleucyl-tRNA synthetases each have a single zinc atom coordinated to ligands contained in the catalytic domain. Isoleucyl-tRNA synthetase has a second, functionally essential, zinc bound to ligands at the C-terminal end of the 939 amino acid polypeptide. Recent evidence suggested that this structure curls back and interacts directly or indirectly with the active site. We show here by X-ray absorption spectroscopy that the average Zn environment contains predominantly sulfur ligands with a Zn−S distance of 2.33 Å. A model with eight coordinated thiolates divided between two $Zn(Cys)_4$ structures best fit the data which are not consistent with a thiolate-bridged $Zn_2(Cys)_6$ structure joining the C-terminal end with the N-terminal active site domain. We also show that zinc bound to the N-terminal catalytic core is important specifically for amino acid binding and utilization, although a direct interaction with zinc is unlikely. We suggest that, in addition to idiosyncratic sequences for tRNA acceptor helix interactions incorporated into the class-defining catalytic domain common to class I enzymes, the architecture of at least some parts of the amino acid binding sites may differ from enzyme to enzyme and include motifs that bind zinc.

A nucleotide binding fold of alternating β-strands and α-helices that contains two characteristic short sequence elements is the common feature that unites all class I tRNA synthetases (Webster et al., 1984; Eriani et al., 1990; Burbaum & Schimmel, 1991; Moras, 1992). This structure is generally located in the N-terminal half of the polypeptide and contains the active site for adenylate synthesis and for transfer of the activated amino acid to the 3′-end of the bound tRNA. Superimposed on this common feature are structural elements that are typically idiosyncratic to the class I enzyme. These include two insertions [designated connective polypeptides 1 and 2 (CP1 and CP2)[1]] into the nucleotide binding fold (Starzyk et al., 1987), where CP1 appears to contain some of the structural elements needed for interactions with the tRNA acceptor helix (Rould et al., 1989). In addition, the C-terminal domain is not held in common by the class I enzymes and is rather poorly conserved in evolution even for the same enzyme (Shiba et al., 1994). For at least some class I enzymes, this nonconserved domain interacts with the tRNA anticodon, which is separated by about 75 Å from the amino acid attachment site at the 3′-end (Rould, et al. 1989; Brunie et al., 1990). A central question is how tRNA interactions with the nonconserved domain are communicated back to the active site.

The presence or absence of bound zinc is another of the idiosyncratic features of class I enzymes. In the class I methionyl-tRNA synthetase, a single zinc atom is bound to a Cys_4 thiolate cluster within the CP1 insertion (Landro & Schimmel, 1993; Fourmy et al., 1993; Xu et al., 1993). Serine replacements of these cysteines generally yielded stable proteins that were devoid of activity, suggesting that the metal is directly or indirectly required for catalytic activity (Landro & Schimmel, 1993). In the related class I isoleucyl-tRNA synthetase, there are two bound zinc atoms, and the d-orbital splitting seen in the visible absorption spectrum of the cobalt-substituted protein was characteristic of thiol ligation (Schimmel et al., 1993a; Xu et al., 1994). In further studies, one of the zinc ligation sites was localized to the C-terminal end of the 939 amino acid polypeptide and included Cys 902, 905, 922, and 925 (Figure 1). Individual serine substitutions of C905 and C925 conferred a zinc-dependent growth phenotype on cells harboring the mutant enzyme as the only source of isoleucyl-tRNA synthetase, while a serine substitution of C902 resulted in an inactive enzyme which could not be rescued by exogenous zinc (Landro & Schimmel, 1994). These results showed that zinc coordinated with the C-terminal segment was essential for function.

Because the C-terminal end of methionyl-tRNA synthetase curls back to the active site in the N-terminal domain and affects the catalytic activity (Kim et al., 1993), we imagined

† This work was supported by Grants GM 15539 (P.S.) and GM 38047 (J.P.-H.) from the National Institutes of Health. J.A.L. is an American Cancer Society Post-Doctoral Fellow, and E.S. is a pre-doctoral trainee of the National Institutes of Health.

* Authors to whom correspondence should be addressed.

⊗ Abstract published in *Advance ACS Abstracts,* November 1, 1994.

[1] Abbreviations: CP1, connective polypeptide 1; CP2, connective polypeptide 2; EXAFS, extended X-ray absorption fine structure; HEPES, 4-(2-hydroxyethyl)-1-piperazineethanesulfonic acid; IleRS, isoleucyl-tRNA synthetase; LB, Luria broth; Tris, tris(hydroxymethyl)-aminomethane; XANES, X-ray absorption near-edge structure; XAS, X-ray absorption spectroscopy.

0006-2960/94/0433-14213$04.50/0

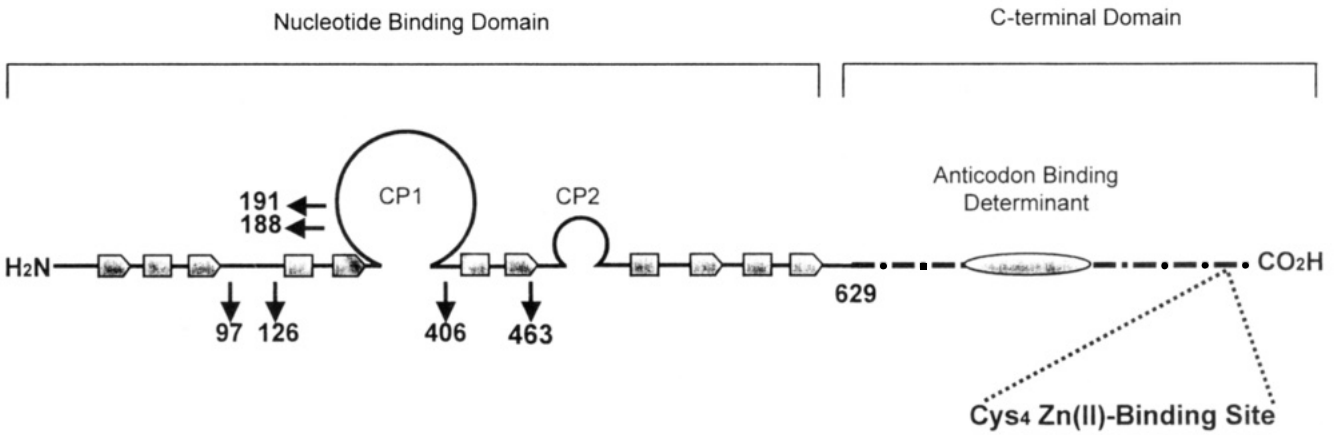

FIGURE 1: Schematic illustration of the class-defining nucleotide binding fold domain which extends to residue 629 and the C-terminal domain of the 939 amino acid polypeptide of *E. coli* isoleucyl-tRNA synthetase. Filled arrows and rectangles designate β-strands and α-helices, respectively. The connective polypeptide CP1 and CP2 insertions are shown as loops. The locations of a previously established Cys_4 C-terminal zinc binding site and the second site investigated here are indicated.

that the zinc-containing C-terminal peptide of isoleucyl-tRNA synthetase might also communicate directly or indirectly with the N-terminal catalytic domain. Zinc-blotting experiments with enzyme fragments showed that the second zinc was bound to the N-terminal domain (Landro & Schimmel, 1994). The most likely ligands were cysteine thiolates at the end of the first half of the nucleotide binding fold (C97 and C126) and at the beginning of CP1 (C188 and C191) (Figure 1). One possibility among others for a direct linkage of the nonconserved C-terminal domain with the class-defining nucleotide binding fold is a Zn_2Cys_6 binuclear cluster, such as that found in the GAL4 transcriptional activator (Marmorstein et al., 1992). Alternatively, the two bound zinc atoms may be sequestered into spatially distinct locations within the protein, even though the structures containing them may interact in some way.

In this work we used extended X-ray absorption fine structures (EXAFS)[1] spectroscopy to determine independently whether the zinc atoms bound to isoleucyl-tRNA synthetase were coordinated to thiol ligands and, if so, whether the zinc atoms shared thiol ligands in a binuclear cluster. We also investigated further the location of and functional significance of the zinc coordinated to the N-terminal domain. In particular, we were interested in determining whether the role of the zinc bound to the N-terminal domain could be ascribed to a particular step in the aminoacylation reaction, or whether it was important only for the overall global folding of the protein.

MATERIALS AND METHODS

X-ray Absorption Measurements. EXAFS samples contained approximately 1 mM isoleucyl-tRNA synthetase with 1 mM zinc in 50 mM HEPES buffer (pH 7.5) in a volume of 50 μL. All samples were prepared with 40% v/v glycerol as a glassing agent, loaded in Lucite cuvettes with 40 μm Kapton windows, and frozen rapidly in liquid nitrogen.

X-ray absorption spectra were measured at the National Synchrotron Light Source, using beamline X9A with a Si(220) double crystal monochromator. The spectra were collected under focused conditions employing an upstream mirror for harmonic rejection. All protein data were measured as fluorescence excitation spectra with a 13-element solid-state Ge detector array, while the data for inorganic model compounds were measured in transmission mode. The Ge detector was run at a total incident count rate of <50 kHz per channel. The windowed count rates (Zn Kα fluorescence) were 1.5−2.0 kHz per channel. Samples were held at 18K in a Displex cryostat during XAS measurements.

EXAFS spectra were measured with 10 eV steps below the edge (9300−9600 eV), ~0.5 eV steps in the edge region (ca. 9630−9700 eV), and 0.05 Å^{-1} steps in the k range 2−13 Å^{-1}. Integration times varied from 1 s in the pre-edge region to 15 s at k = 13 Å^{-1} for a total integration time of approximately 35−40 min/scan. Total exposure time was typically 6 h for protein samples.

Individual scans from each detector channel were examined to confirm the absence of artifacts and averaged to give the final spectra. The EXAFS spectra represent the average of eight scans, each scan being the average of 10−12 channels. For each sample, the total Zn Kα fluorescence counts ranged from ~2 to 3 × 10^6 at k = 13 Å^{-1}. X-ray energies were calibrated by reference to the absorption spectrum of a zinc foil measured at the same time as the data. The first inflection point of the Zn foil was assigned as 9659 eV.

EXAFS background subtraction was accomplished by fitting a first-order polynomial to the pre-edge region and a two-region cubic spline above the edge. Data were converted from energy to k space using $k \approx (2m_e(E - E_0)/h^2)^{1/2}$ with E_0 set at 9675 eV. The resultant EXAFS data were Fourier transformed over the region k = 2.0−12.6 Å^{-1}. The first shell was backtransformed (R = 1.5−2.3 Å for all, except for the ZnS_3N model where R = 1.0−2.3 Å) over the same k range. The resulting EXAFS data (ca. 5 degrees of freedom) were fit to eq 1 by using a nonlinear least squares algorithm.

$$\chi(k) = \sum (N_s A_s(k) S_c / kR^2_{as}) \exp(-2k^2\sigma^2_{as}) \times \exp(-2R_{as}/\lambda) \sin(2kR_{as} + \phi_{as}(k)) \quad (1)$$

In eq 1, N_s is the number of scattering atoms in a shell, $A_s(k)$ is the backscattering amplitude of the absorber−scatterer pair, σ^2 is the mean-square deviation of the absorber−scatterer bond length R_{as}, $\phi_{as}(k)$ is the phase shift, λ is the photoelectron mean free path, and the sum is taken over all shells of scatterers contributing to the EXAFS. The

parameter S_c is the scale factor, which is, in principle, specific to the absorber−scatterer pair. The program FEFF version 3.25 (Rehr et al., 1991) was used to calculate *ab initio* amplitude and phase functions, $A_s(k) \exp(-2R_{as}/\lambda)$ and $\phi_{as}(k)$. Calculations were done for a zinc−nitrogen interaction at 2.05 Å and a zinc−sulfur interaction at 2.35 Å. The scale factor, S_c, and the shift in E_0 relative to 9675 eV were calibrated by fitting compounds of known structure. The models used for calibration were ZnN_4^{2+} for zinc−nitrogen and ZnS_4^{2-} for zinc−sulfur.[2] The optimum values obtained were $S_c = 0.85$ and $\Delta E_0 = 9$ for the zinc−nitrogen model, and $S_c = 1.02$ and $\Delta E_0 = 9$ for the zinc−sulfur model. Subsequent fits to protein and model data were carried out holding the total zinc coordination number fixed at four, while varying the number of nitrogens in steps of 0.25.

For each individual fit, R and σ were allowed to vary for both shells while holding all other parameters fixed. In order to address the question of the detectability of weak nitrogen scattering in the presence of strong sulfur scattering, data were analyzed by the method of Clark (1993). The percent improvement in the mean-square deviation between the data and the fit (P_i) as a function of % sulfur contribution was calculated according to

$$P_i = [(F_{4S} - F_i)/F_{4S}] \times 100 \quad (2)$$

In eq 2, F_{4S} represents the mean-square deviation for a fit of one shell of four sulfurs (two variable parameters), and F_i is the deviation for a two-shell fit including nitrogen contributions (four variables).

EXAFS data for IleRS were measured on two separate samples. A third data set was measured for IleRS with isoleucine bound. These were compared with EXAFS spectra for zinc binding peptides having $Zn(Cys)_4$, $Zn(Cys)_3His$, and $Zn(Cys)_2(His)_2$ environments and for the inorganic model $Zn_2S_6^{2-}$ measured under comparable conditions (Clark, 1993; K. Clark, D. L. Tierney, K. Govindaswamy, E. Gruff, C. Kim, J. Berg, S. A. Koch, and J. E. Penner-Hahn, unpublished data).

Site-Directed Mutagenesis and Complementation Assays. Single-stranded DNA was isolated from the IleRS-encoding pKS21 phagemid (donated by Dr. Kiyotaka Shiba) and subsequently was used as a template for site-directed mutagenesis using the Amersham oligonucleotide mutagenesis system. Mutagenized phagemid was transformed into *Escherichia coli* K12 strain MV1184 [*ara*, Δ(*lac-proAB*), *rspL*, *thi*, (*φ80 lacZ*δM15)], Δ(*srl-recA*) 306::Tn*10*(tet^r)/F′ (*traD36*, *proAB*$^+$, *lacI*^{q}, *lacZ*DM15), and the identities of the mutations were established by DNA sequence analysis using the Sequenase system (United States Biochemical). The activities of mutant enzymes *in vivo* were tested using the *E. coli* K-12 null strains IQ843/pRMS711 [Δ*ileS203*::*kan recA56*, *araD139*, Δ(*argF-lac*)*U169*, *rpsL150relA1*, *flb-B5301*, *deoC1*, *ptsF25*, *rbsR*] and the F′ (*lacI*^{q}, *lac*$^+$, *pro*$^+$) derivative IQ844/pRMS711 as described previously (Shiba & Schimmel, 1992).

Enzyme Purification and Assays. Wild-type IleRS was expressed in strain MV1184 harboring phagemid pKS21 and was purified as described (Shepard et al., 1992). *In vivo* substitution of cobalt(II) (Aldrich Chemicals) was achieved by the method of Xu et al. (1993), and the cobalt-substituted protein was purified as above. Mutant proteins were grown in Luria broth (LB) in one of the two *ileS* null strains (see above) and purified by the same procedure used for the wild-type enzyme, except that the mutants were further purified using 20-μm phenyl ether resin (PerSeptive Biosystems) in 25 mM Tris-HCl (pH 8.0) with a 2.0−0.1 M ammonium sulfate gradient on a Perfusion Chromatography Workstation (PerSeptive Biosystems). Protein was quantitated by Bradford analysis (Bio-Rad) with bovine serum albumin (Sigma) as a standard or by active site titration (Fersht et al., 1975).

Isoleucine-dependent ATP-^{32}PPi (NEN) exchange assays were performed in 25 mM K^+-HEPES buffer (pH 7.5) containing 5 mM $MgCl_2$, 10 mM KF, 0.1 mM EDTA, and BSA (100 μg/mL) as described by Kim and Schimmel (1992) at a fixed ATP concentration and PPi concent ration (2 mM of each) and a variable isoleucine concentration of 5−250 μM. The ATP-dependent exchange reactions were done at a fixed concentration of 400 μM isoleucine and varied ATP concentration from 0.1 to 5 mM.

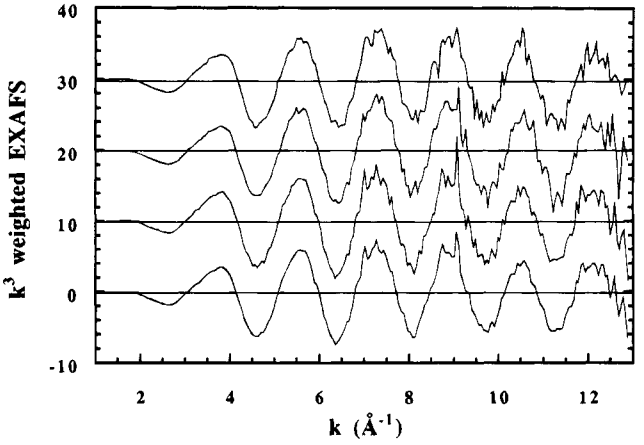

FIGURE 2: EXAFS plots (k^3 weighted) for *E. coli* isoleucyl-tRNA synthetase. From top to bottom the spectra are, respectively, IleRS + 2 mM isoleucine, IleRS sample 2, IleRS sample 1, and the average of the two samples. The spectra have been plotted on the same scale and offset vertically to provide clarity.

RESULTS

X-ray Absorption of Isoleucyl-tRNA Synthetase Shows Primarily Sulfur Ligation. From the background-subtracted data for all three samples of IleRS and the average of two samples, it is clear that the EXAFS amplitude and frequency are reproducible (Figure 2). Curve-fitting results for the individual data sets are summarized in Table 1. Because the individual data sets for IleRS gave similar structural results, they were averaged to obtain a better signal to noise ratio. Comparison of the EXAFS (Figure 2) and the Fourier transforms (Figure 3) with model compounds (data not shown) suggests that the average coordination sphere of the two zinc sites is most consistent with sulfur ligands, with the possibility of a minor nitrogen contribution. Because the EXAFS amplitude associated with sulfur backscattering makes detection of small scatterers difficult, an average $ZnS_{3.5}N_{0.5}$ environment is possible.

In order to clarify this question, a "synthetic" $ZnS_{3.5}N_{0.5}$ model was constructed by calculating the average of the EXAFS data for the $Zn(Cys)_4$ and $Zn(Cys)_3His$ peptide

[2] ZnN_4^{2+} model, the tetrafluoroborate salt of zinc (*N*-methylimidazole)$_4$; ZnS_4^{2-} model, the tetraethylamonium salt of tetrakis(2-phenylbenzenethiol) zinc(II); $Zn_2S_6^{2-}$ model, the tetraphenylphosphonium salt of tetrakis(benzenethiol)di(μ-benzenethiol−Zn(II)).

Table 1: Results of X-ray Absorption Spectroscopy on *E. coli* Isoleucyl-tRNA Synthetase[a]

	S			N		
sample	CN[b]	R_{ab}[c]	σ^2 [d]	CN	R_{ab}	σ^2
enzyme (sample 1)	4.0	2.33	4.0			
	3.5	2.33	3.8	0.5	2.17	0.0
enzyme (sample 2)	4.0	2.33	3.7			
	3.5	2.33	3.5	0.5	2.16	0.0
enzyme + isoleucine	4.0	2.33	4.0			
	3.5	2.33	3.4	0.5	2.17	0.0
$Zn_2S_6^{2-}$ model	4.0	2.36	8.6			

[a] The fits shown are for filtered first-shell data. Fits to the unfiltered data give similar results. [b] Total zinc coordination number CN was held fixed at 4, and sulfur coordination was varied between 4.0 and 3.5. [c] Average absorber−scatterer bond length in angstroms. [d] Mean-square deviation in absorber−scatterer bond length in units of 10^{-3} Å^2.

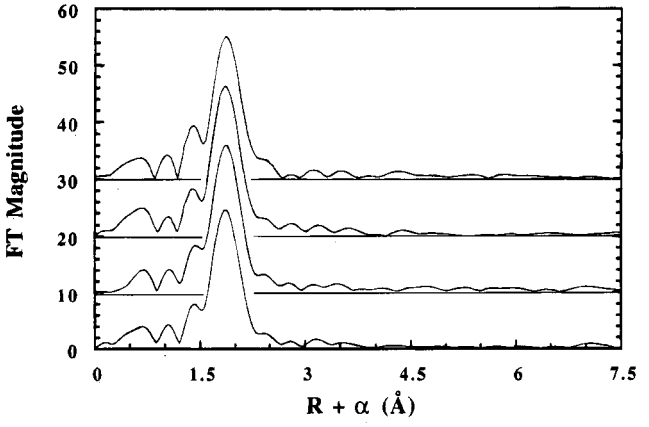

FIGURE 3: Fourier transforms of the EXAFS spectra of isoleucyl-tRNA synthetase. The spectra appear in the same order as given in Figure 2 and have also been offset for clarity.

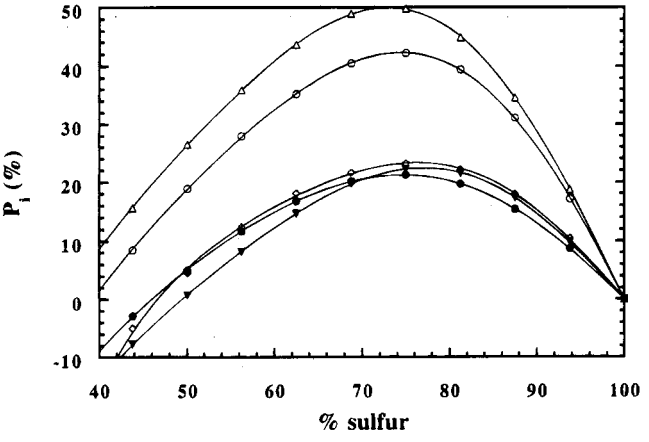

FIGURE 4: Percent improvement (P_i) in the root mean-square deviation of the data and the fit as a function of the fraction of nitrogen scatterers included in the fit. Improvement calculated relative to the fit obtained using a ZnS_4^{2-} model. The total Zn coordination number was held fixed at 4. The five plots correspond to the following: ZnS_3N model peptide (open triangles), calculated $ZnS_{3.5}N_{0.5}$ (open circles), ZnS_4 peptide (open diamonds), IleRS (filled circles), and IleRS + 2 mM isoleucine (inverted filled triangles).

models. The resulting EXAFS was then subjected to the same fitting analysis as the data for the models and for the protein. In each case, a plot of percent improvement (P_i) (Clark, 1993) versus % sulfur took the form of an inverted parabola (Figure 4). The maximum P_i is dependent on the actual amount of sulfur contribution to the observed EXAFS,

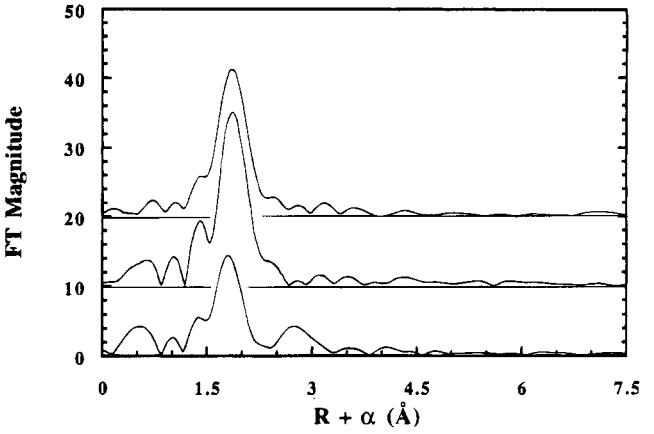

FIGURE 5: Fourier transforms of k^3-weighted EXAFS data for IleRS (top), IleRS + 2 mM isoleucine (middle), and the $Zn_2S_6^{2-}$ model (bottom). These transforms represent a pseudoradial distribution function centered around Zn, shifted by $\alpha \cong -0.4$ Å due to the EXAFS phase shift (eq 1).

increasing from ca. 15% for an all-sulfur environment to approximately 35% for the calculated $ZnS_{3.5}N_{0.5}$ and nearly 50% for three sulfurs and one nitrogen. The % sulfur corresponding to the maximum improvement and the breadth of the curve are also dependent on the amount of sulfur present, though to a lesser degree.

The maximum P_i for all of the enzyme spectra is 20−25%, which occurs at about 80% sulfur (Figure 4). This value is intermediate between the authentic S_4 peptide and the calculated $S_{3.5}N_{0.5}$ model. We conclude that S_4 is the most likely coordination for each of the two zinc atoms, but we cannot rule out the possibility of one S_4 site and one which is S_3N. The best fit results for the one- and two-shell fits for the different spectra of isoleucyl-tRNA synthetase are summarized in Table 1. Although the low-Z scatterer has been modeled as nitrogen in all of the fits, EXAFS cannot distinguish between N and O scattering. Replacing N with O in all of the fits has no effect on the fit results, aside from a 0.03-Å decrease in the apparent Zn−(O/N) distance due to the larger phase shift for O relative to N.

Absence of a Detectable Zn−Zn Interaction. The FTs for IleRS, for IleRS with bound isoleucine, and for inorganic $Zn_2S_6^{2-}$ (which is similar in structure to the thiolate-bridged site in GAL4) show that the principal frequencies are the same for each (Figure 5). However, the FT of $Zn_2S_6^{2-}$ shows outer-shell scattering, corresponding to a Zn−Zn interaction at 3.25 Å. This interaction is not apparent, above the noise level, in the spectrum for either the free enzyme or the enzyme with bound substrate.

Defective Mutant Enzymes Created by Point Substitutions of Thiols in N-Terminal Domain. We showed previously that a zinc binding site is within the first 241 amino acids of the N-terminal domain (Landro & Schimmel, 1994). The likely candidates for thiol coordination in this region are located at C97, 126, 188, and 191. Individual serine replacements of each of these cysteines were created and tested in IQ843 and IQ844 null strains, which contain a complete ablation of the gene-encoding isoleucyl-tRNA synthetase and which are maintained by the IleRS-encoding plasmid pRMS711 (Shiba & Schimmel, 1992). This plasmid has a temperature-sensitive replicon which prevents it from replicating at 42 °C and also encodes the gene-conferring

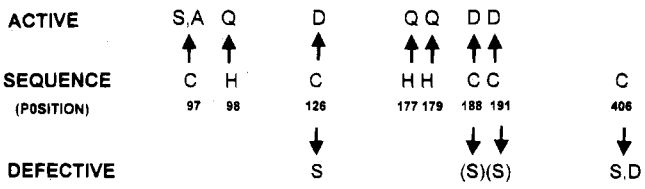

FIGURE 6: Complementation phenotypes of point mutants expressed in the IQ843 and IQ844 null strains (see Materials and Methods). The defective C188S and C191S mutants are indicated in parentheses because the defectiveness of each was different in the two *ileS* null strains as explained in the text.

chloramphenicol resistance (Cm^r). Mutant enzymes expressed from a second, compatible plasmid (pKS21) that harbors a selectable ampicillin-resistance (Amp^R) marker are tested for their ability to rescue a null strain at 42 °C. In this way, the ability of the mutant enzymes alone to support cell growth was determined.

The expression of *ileS* from plasmid pKS21 is under the control of the *lac* promoter, and the tester strains IQ843 and IQ844 differ only in that IQ844 harbors an F′ episome which over expresses the *lac* repressor (Shiba & Schimmel, 1992). In theory, higher levels of the repressor should reduce the "leakiness" of expression of isoleucyl-tRNA synthetase from the inducible *lac* promoter, in the absence of the IPTG inducer. We found that a C97S and C97A replacement yielded active enzyme *in vivo*, which complemented both null strains (Figure 6). However, the C126S mutant was defective. Western blot analysis of this mutant expressed in strain MV1184 showed no detectable protein above the background level expressed from the chromosomal copy of *ileS*, suggesting that the protein was unstable *in vivo*. Because aspartate is a surrogate ligand for zinc (Vallee & Auld, 1993), we also tested a C126D mutant enzyme. The C126D substitution yielded an active enzyme, consistent with the possibility that C126 was a ligation site for zinc.

Similarly, the C188S mutant did not complement in IQ843 null strain, although it did accumulate *in vivo*, suggesting that it was not defective in folding. Curiously, the same mutant showed weak complementation (poor growth phenotype) of the IQ844 null strain. Complementation of both strains was achieved with the C188D substitution. Although the C191S mutant enzyme complemented the IQ843 null strain, growth of these cells was noticeably retarded. In addition, the C191S mutant enzyme did not complement the IQ844 null strain. [Although we can speculate, we do not know why the C188S and C191S mutants behave differently in the two null strains, but in each case the collective data with the two strains demonstrate a defective phenotype (no growth or poor growth, depending on the tester strain used).] The growth defects were removed with the C191D mutant enzyme. Thus, for C126, 188, and 191, serine replacements result in a defective enzyme, and in all three cases, a normal phenotype is restored by making a Cys→Asp substitution.

Because of the possibility of a nitrogen ligand at one of the zinc binding sites, we also investigated histidine as a potential ligand. For this purpose, we considered those histidine residues which are proximal in the sequence to C97, 126, 188, and 191. H98 is conserved among all sequenced isoleucyl-tRNA synthetases, while H177 and H179 are not conserved. Single H98Q and H98A replacements gave mutant enzymes which sustained cell growth as well as wild-type enzyme. We also tested H177Q and H179Q mutant

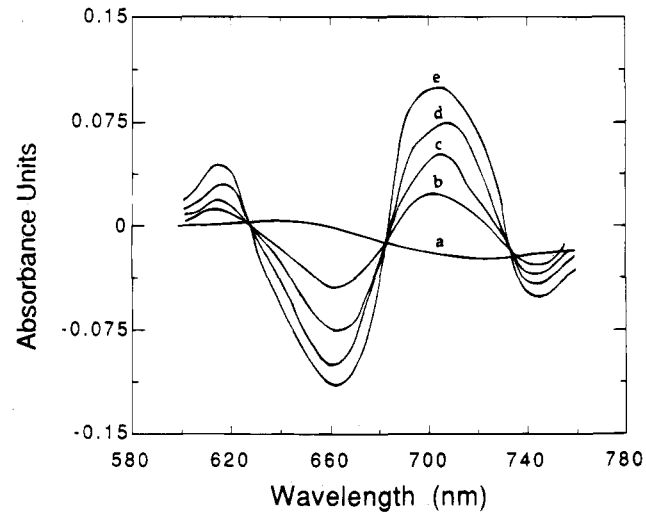

FIGURE 7: Titration of Co(II)-substituted isoleucyl-tRNA synthetase. Changes in the visible absorption spectrum of IleRS [170 μM (85% Co-substituted as determined by atomic absorption spectroscopy)] were measured in 25 mM HEPES (pH 7.5) and 50 mM NaCl using a Beckman DU-64 spectrophotometer. The visible absorbance spectrum of the protein was recorded, set of zero, and then monitored during the incremental addition of isoleucine to the cuvette. The difference spectra changed according to the equivalents of isoleucine added (a, 0.0; b, 0.25; c, 0.50; d, 0.75; and e, 1.0).

enzymes, and these also appeared equivalent to the wild-type enzyme in their ability to support cell growth. Thus, unless zinc ligation to a nitrogen of H98, 177, or 179 is not important for activity, the experiments give no evidence for participation of any of these histidines in zinc binding.

Bound Isoleucine Perturbs UV−Visible Spectrum of Cobalt-Substituted Enzyme. Substitution of native Zn(II) for Co(II) was achieved *in vivo* by growth of strain JM109 harboring the pKS21 plasmid (which encodes wild-type isoleucyl-tRNA synthetase) in LB media that was passed twice over a Chelex-100 resin (Bio-Rad Laboratories) to remove endogenous metals. The media was subsequently supplemented with Co(II) (Aldrich Chemicals) and other essential metals (Xu et al., 1993). Atomic absorption analysis [Northern Analytical Laboratory (Merrimack, NH)] of the enzyme purified from cells grown in this manner contained 0.91 mol of Co(II)/mol of protein and exhibited a UV−visible absorption spectrum having maxima at 365 nm (ϵ = 5500 M^{-1} cm^{-1}), 618 nm (ϵ = 705), 688 nm (ϵ = 960), 712 nm (ϵ = 940), and 728 nm (ϵ = 940). As indicated earlier, this spectrum is characteristic of tetrahedral or near-tetrahedral coordination to predominantly sulfur ligands (Schimmel et al., 1993a).

A difference absorption spectrum of 170 μM Co(II)−IleRS is observed in direct proportion to the amount of isoleucine added, up to a stoichiometric equivalence of enzyme active sites (Figure 7). Amino acid addition causes a red shift in the spectrum with isobestic points occurring at 621, 648, and 730 nm. [Because the enzyme concentration used is more than 10 times the K_m for isoleucine (see below), we cannot calculate a dissociation constant from these data.] A similar change could also be produced by the addition of valine (data not shown). However, the concentration of valine required to produce a similar perturbation (1 mM) was greater than twice the K_m (400 μM), reflecting the 100-fold higher K_m for valine relative to isoleucine. The addition of either ATP or $tRNA^{Ile}$ produced no change in the absorption spectrum.

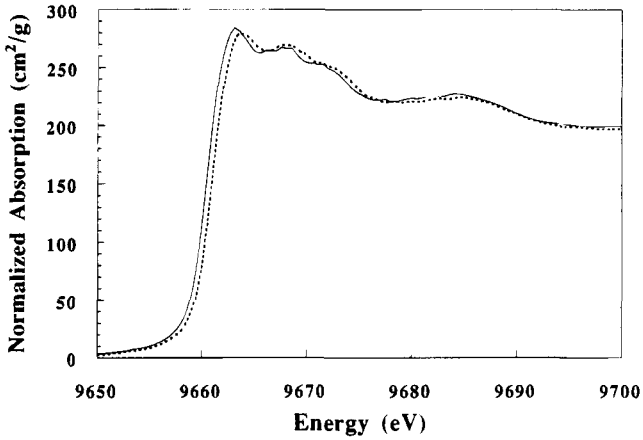

FIGURE 8: Normalized XANES spectra for IleRS with (dashed line) and without (solid line) 2 mM isoleucine. The spectra are plotted on the same scale.

To determine the structural consequences of these spectral changes, X-ray absorption spectra were measured for Zn(II)–enzyme samples in the presence and absence of 2 mM isoleucine. The normalized X-ray absorption near-edge structure (XANES) spectra for free IleRS show a slight shift (approximately 0.5 eV) in the edge energy on binding of isoleucine (Figure 8). Also apparent is a small decrease in the principal absorption maximum. However, there is no observable change in the Zn–S distance, Debye–Waller factor, or apparent percent of sulfur for the different samples.

Kinetic Analysis of Mutant Enzymes Shows Role of N-Terminal Zinc Binding Site in Amino Binding and Utilization. We investigated the kinetic behavior of the mutant enzymes in the isoleucine-dependent ATP-PPi exchange reaction to determine whether the spectral perturbation of the Co(II)-substituted enzyme upon binding of isoleucine was correlated with an effect on the kinetic parameters for amino acid activation by enzymes which had substitutions at the presumed metal coordination site.

The C126D, C188S, and C191S Zn(II)–enzymes were purified (see Materials and Methods), and their kinetic behavior was investigated in the isoleucine-dependent ATP-PPi exchange reaction. The metal content of these enzymes was also investigated by atomic absorption analysis and by the previously described metal ion titration using 4-(2-pyridylazo)resorcinol and *p*-(hydroxymercuri)phenylsulfonate (Landro & Schimmel, 1993). With the C188S and C191S mutant proteins, the K_m for ATP was changed little, and with the C126D enzyme there was a small elevation (2.5-fold). In contrast, the K_m for isoleucine was raised 5–9-fold for the C188S and C191S enzymes, and the k_{cat}/K_m for amino acid activation was reduced by 150- and 105-fold, respectively, for the these two mutants (Table 2). The metal content of each of these enzymes is reduced approximately 50% from that of the wild-type enzyme, although we cannot determine whether the low activity of the C188S and C191S is due to a few molecular species with two zinc atoms bound (weakly) or whether the single zinc-containing species is marginally active. The kinetic parameters were also changed, but far less so, with the C126D mutant enzyme.

Table 2: Kinetic Parameters for Amino Acid Activation for Wild-Type and Mutant Enzymes with Altered Metal-Binding Sites at pH 7.5 and 25 °C

enzyme	k_{cat} (s^{-1})[a]	K_m Ile (μM)	k_{cat}/K_m (relative)	K_m ATP (mM)	Zn content[b] (% wild type)
WT	27.1	5.2	1.0	0.54	100
C126D	10.5	6.1	0.33	1.35	60
C188S	1.7	45.4	0.007	0.75	35
C191S	1.4	27.3	0.01	0.77	60

[a] The k_{cat} values presented are average values determined for K_m Ile (at fixed [ATP]) and for K_m ATP (fixed [Ile]). [b] Metal content is presented as % wild type and represents results obtained from PAR/PMPS analysis and atomic absorption analysis.

DISCUSSION

The curve-fitting results for the X-ray absorption experiments favor an average of 3.5 ± 0.5 sulfur scatterers per zinc atom. Due to difficulty of detecting weak Zn–(N/O) scattering in the presence of strong Zn–S scattering, it is difficult to rule out the possibility that there are a total of seven thiolates and one low Z ligand per two zinc ions. However, the EXAFS data appear most consistent with ZnS_4 coordination for both sites. For example, the shape of the P_i curve and its maxima are most consistent with all-sulfur ligation. In two-shell fits to the data for IleRS, both with and without substrate, σ^2 for the nitrogen shell refined to zero. The value of σ^2 represents the mean-square deviation in the average bond length and is a measure of relative disorder. A refined value of zero is physically unreasonable and implies either that a shell's coordination number is too low or that the atomic number of the scatterer is wrong. That is, a nitrogen scatterer can be made to "look" like a sulfur, at least over a limited k range, by adjusting σ^2 to a very small value. In data that lack a genuine contribution from a nitrogen scatterer (e.g., the ZnS_4 peptide), the value of σ^2 for the nitrogen shell refined to zero in all fits. Physically, this means that the nitrogen shell is being forced to resemble a shell of sulfurs. For a nitrogen to appear sulfur-like, its low k oscillations must be damped and its high k oscillations enhanced. This can be accomplished by making it very rigid, i.e., by giving it very small disorder. The lack of evidence for nitrogen ligands in the X-ray absorption analysis is consistent with the mutagenesis of H98, H177, and H179 as potential nitrogen ligands for zinc, where no phenotype change was observed for glutamine substitutions of each of these histidines (Figure 6).

It is plausible that, by analogy to the methionyl-tRNA synthetase from *E. coli*, the C-terminal end of the enzyme containing one zinc binding site interacts with the N-terminal active site region which contains the other metal site. In principle, this could involve bridging thiolate ligands similar to those seen in the yeast transcription factor GAL4 (Marmorstein et al., 1992). The FTs in Figure 5 clearly show a difference for isoleucyl-tRNA synthetase versus a GAL4-type of model. In particular, there is an obvious Zn–Zn peak well above the noise level for the $Zn_2S_6^{2-}$ model which is not present for isoleucyl-tRNA synthetase. It is possible for a Zn–Zn interaction to be present and not detectable by EXAFS. However, the present data show that any Zn–Zn interaction that is present in isoleucyl-tRNA synthetase must be substantially weaker than those seen in $Zn_2S_6^{2-}$ models. Additional evidence against a GAL4 type of structure in isoleucyl-tRNA synthetase comes from the Zn–S curve-fitting results. In the GAL4 model, the bridging thiolates have longer Zn–S bonds than do the terminal thiolates. This leads to a small increase in the average Zn–S distance and a large increase in the Debye–Waller factor. The observed

distance and Debye−Waller factor for isoleucyl-tRNA synthetase are identical to those seen for mononuclear ZnS_4 centers as distinct from those seen for the GAL4 model. Taken together, these data suggest strongly that the two metal sites in isoleucyl-tRNA synthetase do not interact through a pair of thiolate bridges, as they do in GAL4.

The thiol-containing metal binding sites investigated in this work is assigned to C126, C188, and C191. Serine substitutions at each of these positions gave a defective enzyme while substitution of a surrogate ligand (aspartate) gave active enzyme (Figure 6). C97 is the only other thiol in the N-terminal 241 amino acid segment which could potentially bind zinc in the zinc-blotting assay (Landro & Schimmel, 1994), and it may provide the fourth ligand even though its substitution with serine or alanine does not give a defective complementation phenotype. Alternatively, C126, C188, and C191 may be sufficient to give a signal in the zinc-blotting assay (applied to protein fragments resolved by gel electrophoresis), and if there is a fourth thiol ligand, it may lie outside of the first 241 amino acids. Two possibilities are C406 and C463. However, we found that C406S and C406D substitutions gave enzymes that were unstable (did not accumulate) *in vivo*, while a C463A substitution yielded active enzyme (data not shown).

In the secondary structure model of IleRS, which is based on aligning sequence elements of this enzyme with the known three-dimensional structure of methionyl-tRNA synthetase, C97 and C126 are located between the second β-strand and α-helix of the nucleotide binding fold, while C188 and C191 are contained in the first part of the 277 amino acid insertion known as CP1 (Schimmel et al., 1992; Shiba & Schimmel, 1992). With C97 coordinated to a zinc atom, then C126, C188, and C191 are brought close in space to G94. A G94R substitution was shown earlier to raise the K_m for isoleucine by more than 6000-fold while having little or no effect on the K_m for ATP and $tRNA^{Ile}$ or on the k_{cat} for aminoacylation (Clarke et al., 1988). Although the location of the bound amino acid in the crystal structure of methionyl-tRNA synthetase has not been determined, the co-crystal of tyrosyl adenylate bound to the class I *Bacillus stearothermophilus* tyrosyl tRNA synthetase has been elucidated (Brick et al., 1988). Asp78 in *B. stearothermophilus* tyrosyl tRNA synthetase is close to or at the location of Asp96 of IleRS. The carboxylate of Asp78 in tyrosyl tRNA synthetase is believed to hydrogen bond to the amino group of tyrosine. Thus, the close location of a metal binding site in isoleucyl-tRNA synthetase which is important for amino acid binding and utilization is consistent with previous studies which showed that the same region in this and a related enzyme are at the amino acid binding site.

The lack of a dramatic change in the XANES spectra on the addition of isoleucine (Figure 8) implies that the substrate does not significantly alter the average zinc coordination sphere. The similarity of the P_i curves for IleRS, with and without isoleucine, suggests isoleucine binding does not cause a change in either Zn coordination environment. The changes seen in the visible spectrum of the Co(II)-substituted enzyme (Figure 7) are therefore most likely due to small geometric rearrangements at one or both of the metal sites rather than any change in the ligation of a metal atom.

In another study, deletions in the 277 amino acid CP1 insertion of IleRS were investigated, and the collective results from this analysis showed that the region from residue 231 to residue 377 was dispensable for activity (Starzyk et al., 1987). It was also shown that the protein resulting from deletion of a segment encompassing amino acids 177−276 and thereby including C188 and C191 was inactive. In view of the results reported here, we suggest that one effect of a deletion of residues 177−276 from CP1 was to eliminate a region needed for amino acid interactions.

The four cysteine cluster that binds zinc in methionyl-tRNA synthetase is located entirely within CP1 (Landro & Schimmel, 1993; Fourmy et al., 1993). Individual serine substitutions of each of the four cysteines created a set of four mutant enzymes, three of which accumulated *in vivo* but appeared devoid of activity. The fourth resulted in an enzyme that retained 20% of its catalytic activity *in vitro* and had 0.2 mol of zinc/mol of enzyme. These results collectively suggested that zinc was essential for catalytic activity (Landro & Schimmel, 1993).

The isoleucyl- and methionyl-tRNA synthetases belong to a subset of five of the 10 class I enzymes, which are more closely related to each other than to the other class I enzymes (Hou et al., 1991; Eriani et al., 1991). The other members of this subgroup are cysteinyl-, leucyl-, and valyl-tRNA synthetases. In view of the functional significance of zinc in isoleucyl- and methionyl-tRNA synthetases, it is worth investigation whether at least some of the other members of the subgroup contain bound zinc. The presence of zinc in cysteinyl-, leucyl-, and valyl-tRNA synthetases has not been established, but sites which could bind metal have been suggested for *E. coli* cysteinyl-tRNA synthetase and for *Neurospora crassa*, *Saccharomyces cerevisiae*, and *Saccharomyces douglasii* mitochondrial leucyl-tRNA synthetases (Nureki et al., 1991; Miller et al., 1991). These proposed binding sites are located within CP2 of cysteinyl tRNA synthetase and within CP1 of the three leucyl-tRNA synthetases.

The idiosyncratic structural components of synthetases even within the same class are illustrated by the presence or absence of a metal binding site among other features. For example, the crystal structure of the class I *B. stearothermophilus* tyrosyl-tRNA and *E. coli* glutaminyl-tRNA synthetase contains no bound zinc, even though both enzymes are functional (Bhat et al., 1982; Brick, et al., 1988). Thus, in addition to idiosyncratic sequences recruited into the catalytic domain for recognition of tRNA acceptor helices, synthetases have incorporated different motifs for interactions with different amino acids within the context of the same overall nucleotide binding fold structure. With these considerations in mind, the only part of these enzymes held in common for substrate interactions may be the design of the ATP binding site, which is associated with the nucleotide binding fold itself. The similar binding and orientation of ATP when complexed with tyrosyl- and glutaminyl-tRNA synthetases has been noted previously (Rould et al., 1989).

ACKNOWLEDGMENT

The National Synchrotron Light Source is supported by the U.S. Department of Energy, and beamline X9 is supported by the NIH Division of Research Resources. We thank Professor Jeremy Berg (Johns Hopkins University) for the Zn−peptide models, Professor Stephen Koch (State University of New York at Stony Brook) for the zinc coordination models, and Laura Dickert of PerSeptive

Biosystems for assistance in the use of the Perfusion Chromatography Workstation.

REFERENCES

Bhat, T. N., Blow, D. M., & Brick, P. (1982) *J. Mol. Biol. 158*, 699−709.

Brick, P., Bhat, T. N., & Blow, D. M. (1988) *J. Mol. Biol. 208*, 83−98.

Brunie, S., Zelwer, C., & Risler, J. (1990) *J. Mol. Biol. 216* (2), 411−424.

Burbaum, J. J., & Schimmel, P. (1991) *J. Biol. Chem. 266* (26), 16965−16968.

Clark, K. (1993) Ph.D. Thesis, University of Michigan, Ann Arbor, MI.

Clarke, N. D., Lien, D. C., & Schimmel, P. (1988) *Science 240*, 521−523.

Eriani, G., Delarue, M., Poch, O., Gangloff, J., & Moras, D. (1990) *Nature 347*, 203−206.

Eriani, G., Dirheimer, G., & Gangloff, J. (1991) *Nucleic Acids Res. 19*, 265−269.

Fersht, A. R., Ashford, J. S., Bruton, C. J., Jakes, R., Koch, G. L. E., & Hartley, B. S. (1975) *Biochemistry 14* (1), 1−4.

Fourmy, D., Meinnel, T., Mechulam, Y., & Blanquet, S. (1993) *J. Mol. Biol. 231*, 1068−1077.

Hou, Y.-M., Shiba, K., Mottes, C., & Schimmel, P. (1991) *Proc. Natl. Acad. Sci. U.S.A. 88*, 976−980.

Kim, S., & Schimmel, P. (1992) *J. Biol. Chem. 267*, 15563−15567.

Kim, S., Landro, J. A., Gale, A. J., & Schimmel, P. (1993) *Biochemistry 32*, 13026−13031.

Landro, J. A., & Schimmel, P. (1993) *Proc. Natl. Acad. Sci. U.S.A. 90*, 2261−2265.

Landro, J. A., & Schimmel, P. (1994) *J. Biol. Chem. 269*, 20217−20220.

Marmorstein, R., Corey, M., Ptashne, M., & Harrison, S. H. (1992) *Nature 356*, 408−414.

Miller, W. T., Hill, K. A. W., & Schimmel, P. (1991) *Biochemistry 30*, 6970−6976.

Moras, D. (1992) *Trends Biochem. Sci. 17*, 159−164.

Nureki, O., Muramatsu, T., Suzuki, K., Kohda, D., Matsuzawa, H., Ohta, T., Miyazawa, T., & Tokoyama, S. (1991) *J. Biol. Chem. 266*, 3268−3277.

Rehr, J. J., Mustre de Leon, J., Zabinsky, S. I., & Albers, R. C. (1991) *J. Am. Chem. Soc. 113*, 5135−5140.

Rould, M. A., Perona, J. J., Söll, D., & Steitz, T. A. (1989) *Science 246*, 1135−1142.

Schimmel, P., Shepard, A., & Shiba, K. (1992) *Protein Sci. 1*, 1387−1391.

Schimmel, P., Landro, J. A., & Schmidt, E. (1993a) *J. Biomol. Struct. Dyn. 11*, 571−581.

Schimmel, P., Giegé, R., Moras, D., & Yokoyama, S. (1993b) *Proc. Natl. Acad. Sci. U.S.A. 90*, 8763−8768.

Shepard, A., Shiba, K., & Schimmel, P. (1992) *Proc. Natl. Acad. Sci. U.S.A. 89*, 9964−9968.

Shiba, K., & Schimmel, P. (1992) *Proc. Natl. Acad. Sci. U.S.A. 89*, 1880−1884.

Shiba, K., Suzuki, N., Shigesada, K., Namba, Y., Schimmel, P., & Noda, T. (1994) *Proc. Natl. Acad. Sci. U.S.A. 91*, 7435−7439.

Starzyk, R. M., Webster, T. A., & Schimmel, P. (1987) *Science 237*, 1614−1618.

Vallee, B. L., & Auld, D. S. (1993) *Acc. Chem. Res. 26*, 543−554.

Webster, T. A., Tsai, H., Kula, M., Mackie, G. A., & Schimmel, P. (1984) *Science 226*, 1315−1317.

Xu, B., Krudy, G. A., & Rosevear, P. R. (1993) *J. Biol. Chem. 268*, 16259−16264.

Xu, B., Trawick, B., Kaudy, G. A., Phillips, R. M., Zhou, L., & Rosevear, P. (1994) *Biochemistry 33*, 398−402.